ASME Journal of Applied Mechanics
Online journal at:
https://asmedigitalcollection.asme.org/appliedmechanics

Dengke Guo[1]
School of Aerospace Engineering,
Beijing Institute of Technology,
Beijing 100081, China
e-mail: guodkbit@bit.edu.cn

Dongwei Wang
School of Aerospace Engineering,
Beijing Institute of Technology,
Beijing 100081, China
e-mail: dwfwang@163.com

Yi Chen[1]
Institute of Nanotechnology,
Institute of Applied Physics,
Karlsruhe Institute of Technology,
Karlsruhe 76128, Germany
e-mail: yi.chen@partner.kit.edu

Xiaoning Liu
School of Civil Engineering,
Changsha University of
Science and Technology,
Changsha 410076, China
e-mail: liuxn@csust.edu.cn

Gengkai Hu[1]
School of Aerospace Engineering,
Beijing Institute of Technology,
Beijing 100081, China
e-mail: hugeng@bit.edu.cn

Impedance of Evanescent Modes for Determining Interface States in One-Dimensional Chain

Interface states and edge states in periodic structures have been extensively investigated in the context of topological dynamics over the past decades. In this study, we propose an impedance method based on surface impedance to analyze interface and edge states in one-dimensional (1D) periodic chains. The impedances are defined analytically from the Bloch eigen-modes of the periodic chains. At the interface between two periodic structures, interface states arise at the frequencies where the impedances of the two structures become the same. Likewise, edge states occur when the impedance of the structure matches the boundary impedance. This approach is universal for studying trivial and topological interface and edge states in 1D chain with different types of boundary conditions. We demonstrate this point with three representative examples: a chain comprising two periodic lattices, a chain anchored to ground springs at both ends, and a symmetric chain with interfacial defects. The analysis of topological interface states offers a vivid physical perspective, revealing that the topological interface states are either symmetric or antisymmetric modes. Furthermore, we show that the frequency of the symmetric topological state can be tuned via a single spring at the interface. This finding can be used to design tunable topological devices. [DOI: 10.1115/1.4068253]

Keywords: 1D chain, impedance, interface states, boundary conditions, topological, robustness, tunable

1 Introduction

Interface (edge) waves are modes that are confined to an interface (edge) and decay exponentially away in the media. The initial exploration of surface and interface waves dates back to Rayleigh waves, Love waves, and Stoneley waves in homogeneous media [1]. In periodic structures, interface waves or edge waves can emerge via boundary or interface modification, such as replacing several unit cells or altering the geometry and material parameters [2–6]. These interface states are sometimes referred to as truncation resonances [7] or bandgap resonances [8]. Interface states have been achieved in various physical systems, from photonic crystals (PCs) [9], optical waveguides [10], and graphene [11], to metamaterials [12]. Topological interface or edge states in condensed matter physics [13] have especially garnered significant attention. An unprecedented characteristic of these states is their topological robustness, leading to immune to defects, sharp corners, disorder, and dissipation effects [14]. The associated research has swiftly expanded into the realm of classical waves [15–18], encompassing even zero-frequency floppy modes [19,20] and targeted buckling in lattices that exhibit nontrivial topological polarization [21,22].

In order to understand the physics of interface states in periodic structures, different approaches have been adopted, such as the band structure analysis or using effective-medium theory [6,23] or topological index [24]. The latter one manifests the well-known "*bulk-edge correspondence*," which ensures the existence of interface states between two distinct topological phases. Topological invariants [14], such as winding number, classify different topological phases that are intrinsically linked to the geometrical properties of bulk band [25]. One often-studied example is the Su–Schrieffer–Heeger model for polyacetylene, where an interface state arises when the Zak phase of the occupied band on the one side of the interface differs from that on the other side [26]. However, the topological index solely reflects the bulk property of periodic systems and cannot distinguish the impact of boundary conditions. Techniques involving the addition of an anomalous "cap layer" (a homogeneous layer) [27] or "tuning layer" (unit cells) [28] at the edges of periodic structures have been proposed to control edge states. In fact, even for robust topological interface states, the frequencies are influenced by dislocation [29], defects, and truncations [30] of the unit cell at boundaries.

Multiple studies have delved into the investigation of edge states in 1D discrete structures with different boundary conditions. The existence condition and frequency of the edge state in a 1D diatomic

[1]Corresponding authors.

Contributed by the Applied Mechanics Division of ASME for publication in the Journal of Applied Mechanics. Manuscript received January 27, 2025; final manuscript received March 9, 2025; published online April 7, 2025. Assoc. Editor: Guoliang Huang.

mass-and-spring chain under the free boundary [31] are derived using Rutherford continuants [32] and are generalized to the case with a boundary spring [33]. For the case of alternative spring constants [34], the existence condition for edge states is derived from a characteristic equation by Da-Fonseca [35]. A closed existence condition has been given for a finite 1D chain under general boundary conditions [36]. Recently, the topological index has been adopted to analyze the edge state of a continuum beam with clamped ends [37]. Those methods are limited to studying edge states in their specific structures. A theoretical framework that provides a general understanding of interface states and edge states is still missing.

Generally, interface or edge states can be usually treated as the superposition of propagating Bloch modes and evanescent Bloch modes. Evanescent Bloch modes are ubiquitous in materials [38] and are often indispensable in the continuity condition, as evidenced by the transmission of elastic waves between laminate and homogeneous materials [39,40]. The impedance of these modes is crucial in determining wave reflection and refraction at boundaries or interfaces. Lawrence et al. [41,42] have defined a surface impedance for two-dimensional (2D) PCs, represented by a small matrix that stores the necessary information for calculating reflection and transmission between PCs. They derived the existence conditions for interface modes at an air–PC interface and a three-layer structure with two interfaces. Subsequently, Chan and coworkeres [43,44] established a rigorous relationship between surface impedance and Zak phases in a 1D dielectric structure, enabling the design of interface states between two PCs. The impedance method has emerged as a promising candidate for analyzing interface states in finite periodic structures with general boundary conditions.

In this study, we consider a finite 1D chain with altered masses, separating it into periodic part and boundary part. We analytically derive an impedance for the periodic parts by solving an eigenvalue problem within a unit cell. By leveraging the impedance matching conditions between the periodic parts and boundary parts, we provide analytical solutions for interface states under general boundary conditions. Our further analysis of different examples demonstrates the universality of this method in studying edge and interface states in finite 1D chain. We organize the rest of this article as follows. Section 2 presents an analytical form of the impedance for evanescent Bloch modes. We show in Sec. 3 how to determine edge states in a finite chain from impedance analysis. Section 4 conducts a comprehensive analysis of topological interface states and the impact of defects. A tunable topological functional device through an interfacial spring is demonstrated in Sec. 5. Section 6 concludes the study.

2 Impedance Method for Interface State in One-Dimensional Chain

Impedance matching is an important factor in wave-controlling applications, such as wave mode conversion [45], cloaking [46], and perfect match layer [47], to name a few. Here, we elucidate the principle of the impedance method through a 1D finite chain with an interface at its center. As illustrated in Fig. 1(*a*), the supercell model is composed of two types of lattices with altered masses AB ($m_1 = 1 + \delta m$, $m_2 = 1 - \delta m$, $\delta m = \delta m_1$) and CD ($\delta m = \delta m_2$) connected at node B ($x = 0$). All springs are identical with the same spring constant $K = 1$. Equivalently, the supercell model can be visualized as the interface model shown in Fig. 1(*a*), where AB and CD lattices extend in the $\pm x$ directions but are truncated at $x > 0$ and $x \le 0$, respectively. The remaining sections of the two lattices are connected at the common node B.

For an infinite periodic lattice with lattice constant $a = 1$, we denote the displacement of node α ($\alpha = 1, 2$) in unit cell j as u_α^j (dashed box in Fig. 1(*a*)). Considering Bloch modes ($u_\alpha^j = \tilde{u}_\alpha^0 \exp(\mathrm{i}(\omega t + jka))$) with ω and k being the angular frequency and the wave number, we obtain the following eigenvalue problem:

$$(\mathbf{K} - \mathbf{M}\omega^2)\tilde{\mathbf{u}} = 0,\ \mathbf{K} = \begin{bmatrix} 2 & -1 - \exp(-\mathrm{i}ka) \\ -1 - \exp(\mathrm{i}ka) & 2 \end{bmatrix},\ \mathbf{M} = \begin{bmatrix} m_1 & 0 \\ 0 & m_2 \end{bmatrix}. \tag{1}$$

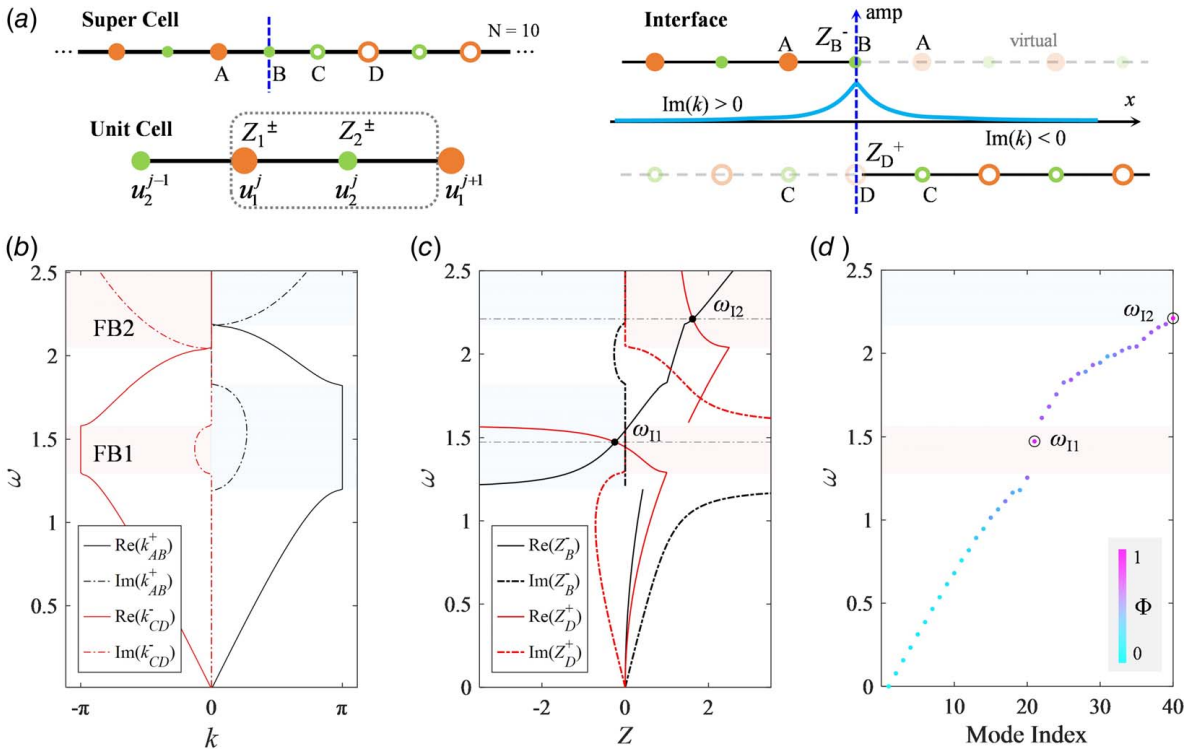

Fig. 1 (*a*) Supercell model, equivalent interface model, and unit cell model, (*b*) complex band structures of AB and CD unit cells, (*c*) impedance Z_B^- and Z_D^+ at the interface, and (*d*) Eigen-frequencies of the supercell model in Fig. 1 (*a*).

where $\tilde{\mathbf{u}}$ represents the displacement eigenvector. The traditional band structure is obtained by solving ω for given k. However, this formula cannot provide information of evanescent Bloch modes in forbidden bands. To better characterize the interface effects, we calculated the complex band structure by solving the wave number k for given ω:

$$\exp(\mathrm{i}k^{\pm}) = \frac{-g \mp \mathrm{sign}(\omega-\omega_{\mathrm{F3}})\sqrt{g^2-4}}{2} \quad g = g_1 g_2 + 2,\ g_1 = (m_1\omega^2 - 2),\ g_2 = (2 - m_2\omega^2),\ \omega_{\mathrm{F3}} = \sqrt{4/(1-\delta m^2)} \tag{2}$$

where $k^{\pm}$ represents the wave number of modes that propagate or amplify in the $\pm x$ directions. For frequencies inside the two forbidden bands: the first forbidden band (FB1 $= [\omega_{\mathrm{F1}},\ \omega_{\mathrm{F2}}]$) and the second forbidden band (FB2 $= [\omega_{\mathrm{F3}},\ +\infty]$) with $\omega_{\mathrm{F1,2}} = \sqrt{2/(1 \pm \delta m)}$, the Bloch modes become evanescent modes and the wave numbers become complex valued. At the central frequency $\omega_c = \sqrt{2/(1-\delta m^2)}$ in FB1, the decay coefficient of the evanescent modes ($c = \mathrm{Abs}[\mathrm{Im}(k^{\pm})]$) reaches its maximum:

$$c_{\max} = \mathrm{Abs}\left[\mathrm{Im}\left\{\ln\left(1 + \frac{1}{m_1} - \frac{1}{m_2} - 2\sqrt{\frac{-\delta m^2}{m_1^2 m_2^2}}\right)\right\}\right] \tag{3}$$

We proceed to define the impedance of the modes by adopting the concept of deformation impedance from vibration systems $Z_\alpha = F_\alpha/u_\alpha$, where F_α denotes the input excitation load acting on node α and u_α is the output displacement [48]. Along this line, the impedance of the lattice at node α is defined as follows:

$$Z_\alpha^{\pm} = \frac{\tilde{f}_{\alpha\beta}}{\tilde{u}_\alpha} = 1 + \left[\frac{1}{(1 + e^{ik^{\mp}})}\right]^{\mathrm{sign}(\alpha-\beta)} \tag{4}$$

where $\tilde{f}_{\alpha\beta} = \tilde{u}_\alpha - \tilde{u}_\beta$ is the force in spring indexed $\alpha\beta$ for the Bloch modes and $Z_\alpha{}^{\pm}$ represents the impedances at node α for eigen-mode that decay away from the interface in $\pm x$ directions with $k^{\mp}$. Due to the parity of node mass in a unit cell, the values of $Z_\alpha{}^{\pm}$ at node α for δm equal to $Z_\beta{}^{\mp}$ at node β for $-\delta m$. By substituting Eq. (2) into Eq. (4), $Z_\alpha{}^{\pm}$ can be expressed as functions of the angular frequency ω. The impedance is complex valued within passbands and becomes real valued within the two forbidden bands.

For an interface state localized at the interface shown by the interface model in Fig. 1(*a*), the displacement field and the force must be continuous across the interface. In order to obtain nontrivial solutions, these two conditions together imply the impedance match condition on the interface. Notice that, the evanescent Bloch modes on each side of the interface must decay away from the interface in opposite directions. We then obtain the condition for interface states, i.e., $Z_B^- = Z_D^+$, with the following form:

$$\left.\frac{(1 + e^{ik^+})}{g_1}\right|_{\delta m=\delta m_1} = \left.\frac{(1 + e^{ik^-})}{g_1}\right|_{\delta m=\delta m_2} \tag{5}$$

By substituting Eq. (2) into Eq. (5), we obtain three general solutions in forbidden bands:

$$\begin{aligned}\omega_{\mathrm{I1}} &= \Gamma + \frac{1}{p}\left[\frac{\sqrt[3]{2}\Xi}{3\Delta} - \frac{\Delta}{3\sqrt[3]{2}}\right] \\ \omega_{\mathrm{I2,3}} &= \Gamma + \frac{1}{p}\left[\frac{(1 \mp i\sqrt{3})\Xi}{3\sqrt[3]{4}\Delta} - \frac{(1 \pm i\sqrt{3})\Delta}{6\sqrt[3]{2}}\right]\end{aligned} \tag{6}$$

with

$$\begin{aligned}c_{12} &= (1 - \delta m_1)(1 + \delta m_1), \\ d_{12} &= (1 - \delta m_2)(1 + \delta m_2), \\ p &= c_{12} + d_{12}, \\ q &= c_{12} d_{12}, \\ \Gamma &= \frac{4p}{3q}, \\ \Xi &= -16p^2 + 12q(p + 3), \\ \Lambda &= 144(-\delta m_1^6 \delta m_2^2 + \delta m_1^4 \delta m_2^4 - \delta m_1^2 \delta m_2^6) + \ldots \\ &\quad 16(\delta m_1^6 + 12\delta m_1^4 \delta m_2^2 + 12\delta m_1^2 \delta m_2^4 + \delta m_2^6) + \ldots \\ &\quad 48(\delta m_1^4 - 10\delta m_1^2 \delta m_2^2 + \delta m_2^4) + 48(\delta m_1^2 + \delta m_2^2) + 16, \\ \Delta &= \sqrt[3]{\Lambda + \sqrt{\Lambda^2 + 4\Xi^3}}\end{aligned}$$

where ω_{I1} in FB1 and ω_{I2} in FB2 represent interface states that arise for small mass connection, i.e., smaller masses are located on the interface ($\delta m_1 > 0$, $\delta m_2 < 0$), while ω_{I2} in FB1 corresponds to interface state for big mass connection ($\delta m_1 < 0$, $\delta m_2 > 0$). Notably, no interface state exists in forbidden bands when δm_1 and δm_2 have the same sign.

To illustrate these solutions, we present a numerical example by setting $\delta m_1 = 0.4$ and $\delta m_2 = -0.2$. The complex band structures for AB and CD unit cells are shown in Fig. 1(*b*), and the impedances for the two lattices are plotted versus angular frequency in Fig. 1(*c*). The two impedances $Z_B{}^-$ and $Z_D{}^+$ match at two frequencies $\omega_{\mathrm{I1}} = 1.473$ in FB1 and $\omega_{\mathrm{I2}} = 2.211$ in FB2. To verify the correctness of the impedance method, we show the calculated eigen-frequencies of the supercell model (Fig. 1(*a*)) by finite element method (FEM) in Fig. 1(*d*). We use a mode concentration factor Φ to identify localized modes, defined as $\Phi = \left(\sum_i^{2N}[1 - u_i^2/\max(u_i^2)]/2N\right)^4$, where u_i represents the displacement of the ith node in supercell and N is the number of unit cells on one side. High Φ values near 1 indicate localized modes, while small values near 0 suggest nonlocalized bulk modes. The supercell model has 40 eigen-modes, among which the two interface states ω_{I1} and ω_{I2} precisely match the frequencies obtained by the impedance method (Fig. 1(*d*)). Unlike the FEM for solving boundary states, the impedance matching method in forbidden bands takes great advantage in elucidating the physical mechanisms of boundary states.

3 Edge State Induced by Boundary Stiffness in One-Dimensional Chain

When infinite chains are truncated to finite sections, edge states may exist at boundaries, depending on mass distributions, boundary conditions, and so on [36]. We utilize the impedance method to build a general framework to address this problem analytically. We study a finite periodic chain connected to grounded springs with stiffness K_b at both ends, as illustrated in Fig. 2(*a*). We remark here that $K_b = 0$ means free boundaries and sufficiently large K_b approximates clamped boundaries. The impedance of the periodic chain at the left end and the right end are denoted as $Z_A{}^+$ and $Z_B{}^-$, respectively. The impedance for the two grounded springs is $Z_b = f_b/u_b = K_b$, where u_b is the displacement of the node and f_b is the force in the boundary spring. By applying the impedance match condition of $Z_b = Z_A{}^+$ and $Z_b = Z_B{}^-$, we derive the frequencies of the edge states at the left (L) and the right (R) end in forbidden bands:

$$\omega_{\Psi 1,2} = \frac{-s_\Psi \pm \sqrt{s_\Psi^2 + 8m_1 m_2(1 - K_b)K_b^2}}{2m_1 m_2(1 - K_b)} \quad (\Psi = L, R) \tag{7}$$

with

$$\begin{aligned}s_L &= (2m_2 + K_b m_1)K_b - 2, \\ s_R &= (2m_1 + K_b m_2)K_b - 2\end{aligned}$$

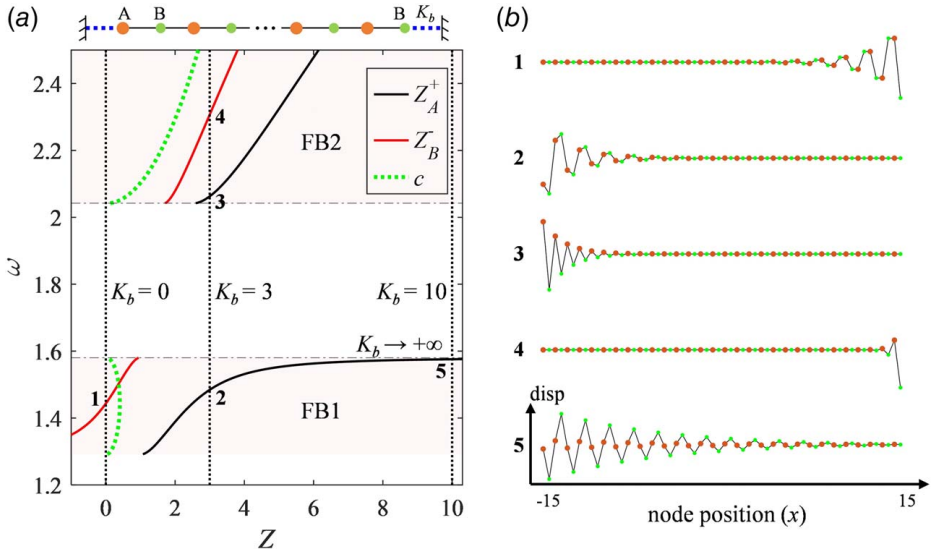

Fig. 2 (*a*) Supercell: AB lattice ($m = -0.2$) with 30 unit cells connected to two grounded springs. The impedances of node A (Z_A^+) and B (Z_B^-) at two ends and the decay coefficient *c*. (*b*) Edge states 1–5.

There exists left edge state in FB1 (ω_{L1}) for $K_b \in (1, +\infty)$ and in FB2 (ω_{L2}) for $K_b \in (2/(1+\delta m), +\infty)$. Right edge states occur in FB1 (ω_{R1}) and FB2 (ω_{R2}) for $K_b \in [0, 1)$ and $(2/(1-\delta m), +\infty)$, respectively. We present an example of a finite chain ($\delta m = 0.2$, $N = 30$) to validate the analysis. Impedances at the left end (Z_A^+) and the right end (Z_B^-) are plotted in Fig. 2(*a*). The dashed line at $K_b = 0$ intersects with Z_B^- at point 1 ($\omega_{R1} = 1.443$) in FB1, indicating an edge state at the right end. This is confirmed by mode 1 in Fig. 2(*b*). When $K_b = 3$, three surface states emerge at points 2–4 ($\omega_{L1} = 1.484$, $\omega_{L2} = 2.063$, and $\omega_{R2} = 2.307$), among which mode 2–3 are edge states at the left end, while mode 4 corresponds to the right end. When the chain is clamped ($K_b \to \infty$), the impedance matches at the right end in FB1, similar to mode 5 ($K_b = 10$, $\omega_{L1} = 1.576$), where the displacement of the node connected to the boundary spring is suppressed.

4 Topological Interface State and Defects in One-Dimensional Symmetric Chain

Recently, Zhang et al. reported a class of "strain topological metamaterials," capable of achieving winding numbers of 0 and 1. Those topological properties are apparent only in higher-order ("strain") coordinates but hidden in the standard coordinates [49]. By employing the impedance method, we can analyze topological interface states without relying on winding numbers and the "strain" coordinates. This approach is also suitable for analyzing the robustness of the topological states and the impacts of defects.

We first analyze the topological interface state in a defect-free model in Fig. 3(*a*), which is equivalent to the interface model in Fig. 1(*a*), under the assumption $\delta m_2 = -\delta m_1 = \delta m$. Topological interface states arise due to different topological numbers of the left and the right parts [50,51]. Three general solutions of Eq. (7) are the angular frequencies of the topological interface states, i.e., $\omega_{I1} = \sqrt{2/(1-\delta m^2)}$ in FB1 and $\omega_{I2} = \sqrt{(3+\sqrt{1+8\delta m^2})/(1-\delta m^2)}$ in FB2 for $\delta m < 0$ (meaning two small masses at the interface), and $\omega_{I3} = \sqrt{(3-\sqrt{1+8\delta m^2})/(1-\delta m^2)}$ in FB1 for $\delta m > 0$ (meaning two big masses at the interface). Additionally, two degenerated edge states $\omega_{E4} = \omega_{I1}$ exist at free ends. As illustrated in Fig. 3(*c*), the frequencies obtained from the impedance method (black marker) agree well with the supercell result (color coded by Φ).

The impedance method is also capable of studying the impact of defects on the topological states. We consider a defects model as shown in (Fig. 3(*a*)), where the defects are two masses with $m_{d1} = (1+\delta m)\xi/\eta$ and $m_{d2} = (1+\delta m)\xi\eta$. The impedance analysis is schematically shown in Fig. 3(*b*). Due to the symmetry, the impedance on the left side (Z_B^-) of the interface layer equals to that on the right (Z_B^+) and are both denoted as Z_I. Thus, the dynamic equation for the interface layer can be written as follows:

$$(\mathbf{H} - Z_I \mathrm{I})\mathbf{u} = 0, \ \mathbf{H} = \begin{bmatrix} 1 - m_{d1}\omega^2 & -1 \\ -1 & 1 - m_{d2}\omega^2 \end{bmatrix} \tag{8}$$

The two solutions for Z_I are as follows:

$$Z_{I1,2} = \mathrm{Eig}(\mathbf{H}), \ Z_{I1} < Z_{I2} \tag{9}$$

where Z_{I1} and Z_{I2} are the boundary impedance for the anti-phase and in-phase mode ($\mathbf{u}$), respectively.

By applying the impedance match condition: $Z_{I1} = Z_B^+$, $Z_{I2} = Z_B^+$, we get the solutions of symmetric and antisymmetric edge states at the interface. Here, we focus on states within FB1 and select states 1 ($\delta m = -0.4$, $\omega_{I1} = 1.543$) and 2 ($\delta m = 0.4$, $\omega_{I2} = 1.332$) as benchmarks to analyze the impact of defects (Fig. 3(*d*)). As η increases (with $\xi = 1$), which implies an enlargement of the mass discrepancy on the interface, the topological bands persist for both small and large mass connections, while they are shifted downward and upward, respectively. Notably, as ξ increases (with $\eta = 1$), which signifies an increase in the overall interfacial mass, a new interface state arises for small mass connection, while a decrease of ξ is required for large mass connection. Conversely, the states might be eliminated when alter ξ in the opposite directions. Impedances on the interface (Z_B^+, Z_I) are depicted in Fig. 3(*e*). The intersection points 5 ($\eta = 8$, $\omega_{I5} = 1.206$) and 8 ($\eta = 3$, $\omega_{I8} = 1.543$) are from Z_{I2} and Z_{I1} for small and large mass connections, respectively, and they converge to states 1 and 2 when $(\eta, \xi) = (1, 1)$. Interestingly, due to the frequency of state 8 (ω_{I8}), which is occasionally similar to that of state 4 (ω_{E4}), the supercell exhibits three modes at $\omega = 1.543$, among which are two degeneracy mixed modes localized at both interface and edges, as shown by mode 8 in Fig. 3(*f*) and a pure edge state on free ends, similar to mode 1 in Fig. 2(*b*). The antisymmetric ($\omega_{I6} = 1.228$, $\omega_{I9} = 1.432$) and symmetric states ($\omega_{I7} = 1.312$, $\omega_{I10} = 1.741$) are generated by the change of overall mass on the interface. Notice that, all interface

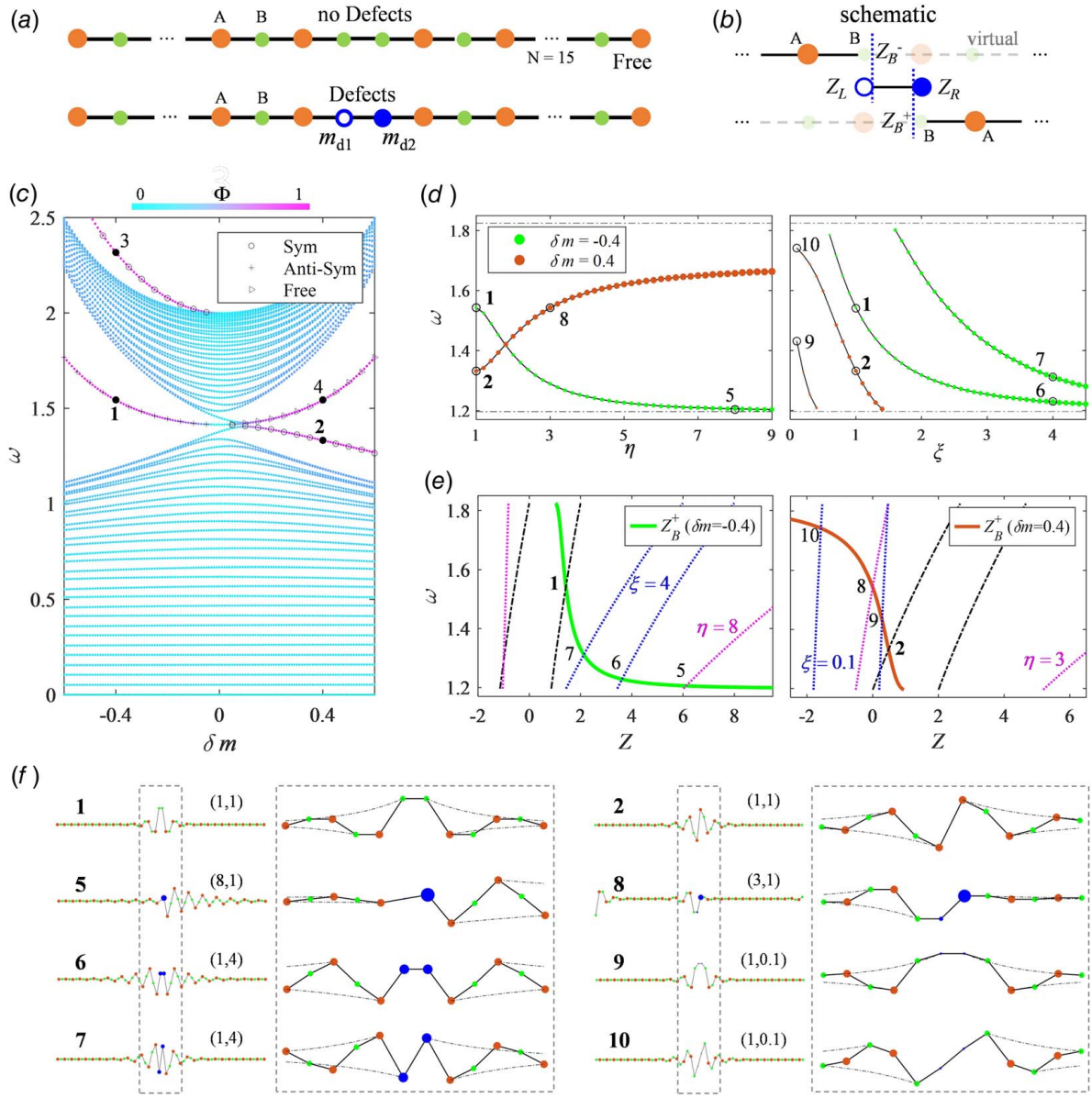

Fig. 3 (*a*) Supercell of no defects and defects model. (*b*) Schematic of the impedance method for defects model. (*c*) Topological bands by impedance method and finite element method. (*d*) The influence of defect parameters η (left) and ξ (right) on interface states for $\delta m = -0.4$ (green markers with points 1, 5, 6, 7) and $\delta m = 0.4$ (maroon markers with points 2, 8, 9, 10). (*e*) The influence of defect parameters on boundary impedances. Left: Impedance Z_I with parameters $(\eta, \xi) = (1, 1)$ (black, dash-dotted line), (8, 1) (magenta, dotted line), and (1, 4) (blue, dotted line) and Impedance Z_B^+ for $\delta m = -0.4$ (green solid line). Right: Impedance Z_I with parameters $(\eta, \xi) = (1, 1)$ (black, dash-dotted line), (3, 1) (magenta, dotted line), (1, 0.1) (blue, dotted line) and impedance Z_B^+ for $\delta m = 0.4$ (maroon solid line). (*f*) Eigen states correspond to 1, 2, 5–10 in (*b*), (*c*), (*d*), and (*e*).

states are eliminated when $\xi < 0.5$ and $\xi > 1.5$ for small and large mass connection cases, respectively. Our analysis on the defect model indicates the topological protection property in certain aspects that the interface state always exists for asymmetric defects within a large parameter range. However, topological interface states are indeed greatly influenced by defects on the interface and even eliminated in some cases.

5 Tuning Topological Interface State Through Interfacial Parameter

Topological insulators constitute a distinct class of advanced waveguides that exhibit exceptionally robust transmission properties, making them suitable for applications in photonic logic [52], advanced vibration isolation [53], energy trapping, or harvesting devices [54]. The development of smart and intelligent metamaterials that possess tunable and active wave dynamics is of considerable interest [55–57]. Recently, a tunable topological functional device has been reported to modulate the topological phase through tuning embedded magnetic springs within the metamaterial [51]. The aforementioned analysis has demonstrated that, in addition to the bulk properties, interface properties can also be used to control the topological states. This will largely reduce the number of required actuating elements.

Here, we consider a topological system with a magnetically tunable spring (as depicted in Fig. 3 of Ref. [51]) at the interface, as illustrated in Fig. 4. Due to the mirror symmetry of the system, the interface spring undergoes either rigid translation (antisymmetric) or telescopic (symmetric) deformation. Therefore, the impedance of the spring is $Z_I = 0$ or $2K_I$, respectively. With the

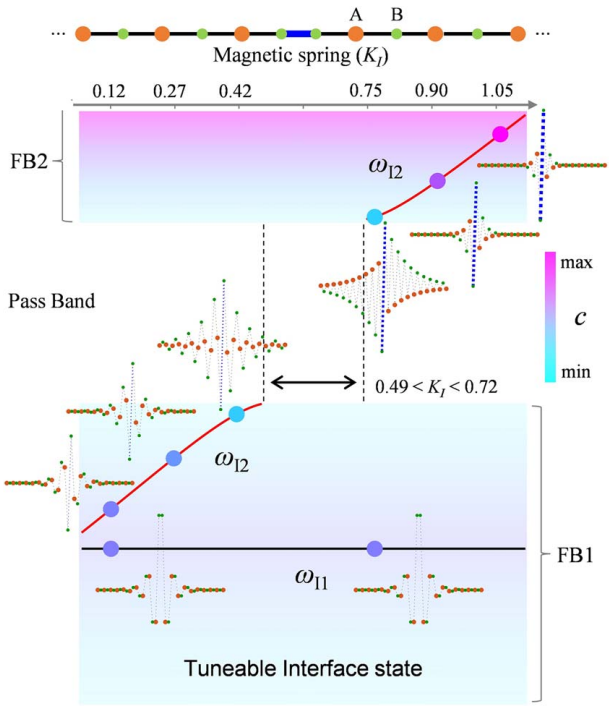

Fig. 4 Tunable topological interface states through an interfacial magnetic spring (K_I). The device is consisted of symmetrically distributed AB type lattice with small mass ($\delta m = -0.4$) at the interface. Frequencies of interface states with varying K_I and the mode shapes for different K_I values are displayed.

impedance matching condition, we obtain an antisymmetry interface state at ω_{I1} for ${Z_B}^+ = 0$ and a symmetric interface state at ω_{I2} for ${Z_B}^+ = 2K_I$. The angular frequency $\omega_{I1} = 1.543$ of the antisymmetric mode is independent of the interface spring stiffness, as the spring undergoes rigid translation. The frequency of the symmetric mode can be tuned over a large range by varying the stiffness K_I, as shown in Fig. 4. When $K_I \in (0.49, 0.72)$, the symmetric interface state disappears in the passband region. The localization degree of the symmetric state in FB1, determined by the decay coefficient c, decreases with the increase of K_I. In FB2, the decay coefficient increases significantly and the interface states can be highly localized.

6 Conclusion

In this article, we proposed an impedance method for studying interface states and edge states in finite one-dimensional diatomic mass-and-spring chains. The key idea is to consider the impedance of finite periodic lattice and the impedance of boundary or interface parts separately. Interface and edge states are derived by considering the impedance matching of different parts. This method is applicable to typical boundary conditions, e.g., boundary spring, attached mass, and interface layer. Three situations are theoretically analyzed and numerically validated, including the interface states between two finite periodic lattices, the edge states at two ends of periodic lattices under different boundary conditions, and the topological interface states between two distinct topological phases. In particular, it is shown that the symmetric topological interface states can be tuned over a wide frequency range by varying the stiffness of a single interfacial spring, enabling design tunable topological devices. The impedance method provides a robust tool to investigate interface and edge states and can be potentially generated to higher dimensions.

Acknowledgment

Discussion from Quan Zhang is acknowledged.

Funding Data

- The National Natural Science Foundation of China (Grant Nos. 12202054, 11632003, 11972083, 11991030, and 12372089).

Conflict of Interest

There are no conflicts of interest.

Data Availability Statement

The authors attest that all data for this study are included in the paper.

References

[1] Achenbach, J. D. D., and Thau, S. A., 1974, "Wave Propagation in Elastic Solids," ASME J. Appl. Mech., **16**(2), pp. 262–325.
[2] Aono, T., and Tamura, S., 1998, "Surface and Pseudosurface Acoustic Waves in Superlattices," Phys. Rev. B, **58**(8), pp. 4838–4845.
[3] Polo, J. A., and Lakhtakia, A., 2011, "Surface Electromagnetic Waves: A Review," Laser Photonics Rev., **5**(2), pp. 234–246.
[4] Zhou, X. M., Badreddine Assouar, M., and Oudich, M., 2014, "Subwavelength Acoustic Focusing by Surface-Wave-Resonance Enhanced Transmission in Doubly Negative Acoustic Metamaterials," J. Appl. Phys., **116**(19), p. 194501.
[5] Zhao, Y. C., Zhou, X. M., and Huang, G. L., 2020, "Non-Reciprocal Rayleigh Waves in Elastic Gyroscopic Medium," J. Mech. Phys. Solids, **143**, p. 104065.
[6] Wei, Y., Chen, Y., Cheng, W., Liu, X. N., and Hu, G. K., 2024, "Rayleigh Surface Waves of Extremal Elastic Materials," J. Mech. Phys. Solids, **193**, p. 105842.
[7] Al Ba'ba'a, H. B., Willey, C. L., Chen, V. W., Juhl, A. T., and Nouh, M., 2022, "Theory of Truncation Resonances in Continuum Rod-Based Phononic Crystals With Generally Asymmetric Unit Cells," Adv. Theory Simul., **6**, p. 253265314.
[8] Zhang, Q., Chen, Y., Zhang, K., and Hu, G. K., 2020, "Dirac Degeneracy and Elastic Topological Valley Modes Induced by Local Resonant States," Phys. Rev. B, **101**(1), p. 014101.
[9] Huang, X. Q., Xiao, M., Zhang, Z. Q., and Chan, C. T., 2014, "Sufficient Condition for the Existence of Interface States in Some Two-Dimensional Photonic Crystals," Phys. Rev. B, **90**(7), p. 075423.
[10] Bai, R. B., and Suo, Z. G., 2015, "Optomechanics of Soft Materials," ASME J. Appl. Mech., **82**(7), p. 071011.
[11] Zhang, T., and Gao, H. J., 2015, "Toughening Graphene With Topological Defects: A Perspective," ASME J. Appl. Mech., **82**(5), p. 051001.
[12] Zhang, Q., Cherkasov, A. V., Arora, N., Hu, G. K., and Rudykh, S., 2023, "Magnetic Field-Induced Asymmetric Mechanical Metamaterials," Extreme Mech. Lett., **59**, p. 101957.
[13] Hasan, M. Z., and Kane, C. L., 2010, "Colloquium: Topological Insulators," Rev. Mod. Phys., **82**(4), pp. 3045–3067.
[14] Zhen, B., Hsu, C. W., Lu, L., Stone, A. D., and Soljačić, M., 2014, "Topological Nature of Optical Bound States in the Continuum," Phys. Rev. Lett., **113**(25), p. 257401.
[15] Mousavi, S. H., Khanikaev, A. B., and Wang, Z., 2015, "Topologically Protected Elastic Waves in Phononic Metamaterials," Nat. Commun., **6**(1), p. 8682.
[16] Huber, S. D., 2016, "Topological Mechanics," Nat. Phys., **12**(7), pp. 621–623.
[17] Inoue, T., and Murakami, S., 2019, "Topological Band Structure of Surface Acoustic Waves on a Periodically Corrugated Surface," Phys. Rev. B, **99**(19), p. 195443.
[18] Chen, H., Zhang, H. K., Wu, Q., Huang, Y., Nguyen, H., Prodan, E., Zhou, X. M., and Huang, G. L., 2021, "Creating Synthetic Spaces for Higher-Order Topological Sound Transport," Nat. Commun., **12**(1), p. 5028.
[19] Sun, K., Souslov, A., Mao, X. M., and Lubensky, T. C., 2012, "Surface Phonons, Elastic Response, and Conformal Invariance in Twisted Kagome Lattices," Proc. Natl. Acad. Sci. U. S. A., **109**(31), pp. 12369–12374.
[20] Chen, Y., Mcinerney, J. P., Krause, P. N., Schneider, J. L. G., Wegener, M., and Mao, X. M., 2025, "Observation of Floppy Flexural Modes in a 3D Polarized Maxwell Beam," Phys. Rev. Lett., **134**(8), p. 086101.
[21] Wang, A. X., Zhou, Y., and Chen, C. Q., 2023, "Topological Mechanics Beyond Wave Dynamics," J. Mech. Phys. Solids, **173**, p. 105197.
[22] Singhal, A., 2025, "Surface Effects Study: A Continuum Approach From Fundamental Modes to Higher Modes and Topological Polarization in Orthotropic Piezoelectric Materials," ASME J. Appl. Mech., **92**(1), p. 011008.
[23] Zhu, R., Huang, G. L., and Hu, G. K., 2012, "Effective Dynamic Properties and Multi-Resonant Design of Acoustic Metamaterials," ASME J. Vib. Acoust., **134**(3), p. 031006.
[24] Xiao, M., Ma, G. C., Yang, Z. Y., Sheng, P., Zhang, Z. Q., and Chan, C. T., 2015, "Geometric Phase and Band Inversion in Periodic Acoustic Systems," Nat. Phys., **11**(3), pp. 240–244.
[25] Chen, Y., Liu, X. N., and Hu, G. K., 2019, "Topological Phase Transition in Mechanical Honeycomb Lattice," J. Mech. Phys. Solids, **122**, pp. 54–68.
[26] He, Y., and Chien, C. C., 2020, "Non-Hermitian Generalizations of Extended Su–Schrieffer–Heeger Models," J. Phys. Condens. Matter, **33**(8), p. 085501.

[27] Boudouti, E. H. E., Rouhani, B. D., Akjouj, A., and Dobrzynski, L., 1996, "Theory of Surface and Interface Transverse Elastic Waves in N-Layer Superlattices," Phys. Rev. B, **54**(20), pp. 14728–14741.
[28] Hussein, M. I., Hulbert, G. M., and Scott, R. A., 2007, "Dispersive Elastodynamics of 1D Banded Materials and Structures: Design," J. Sound Vib., **307**(3–5), pp. 865–893.
[29] Ammari, H., Davies, B., and Hiltunen, E. O., 2022, "Robust Edge Modes in Dislocated Systems of Subwavelength Resonators," J. London Math. Soc., **106**(3), pp. 2075–2135.
[30] Rosa, M. I. N., Davis, B. L., Liu, L., Ruzzene, M., and Hussein, M. I., 2023, "Material vs. Structure: Topological Origins of Band-Gap Truncation Resonances in Periodic Structures," Phys. Rev. Mater., **7**(12), p. 124201.
[31] Wallis, R. F., 1957, "Effect of Free Ends on the Vibration Frequencies of One-Dimensional Lattices," Phys. Rev., **105**(2), pp. 540–545.
[32] Rutherford, D., 1948, "XXV. Some Continuant Determinants Arising in Physics and Chemistry," Proc. R. Soc. Edinburgh, Sect. A: Math., **62**(3), pp. 229–236.
[33] Puszkarski, H., 1983, "Effect of Surface Parameter on Interband Surface Mode Frequencies of Finite Diatomic Chain," Physica B + C, **115**(3), pp. 367–375.
[34] Al Ba'ba'a, H., Nouh, M., and Singh, T., 2019, "Dispersion and Topological Characteristics of Permutative Polyatomic Phononic Crystals," Proc. R. Soc. A, **475**(2226), p. 20190022.
[35] Da-Fonseca, C. M., 2007, "The Characteristic Polynomial of Some Perturbed Tridiagonal k-Toeplitz Matrices," Appl. Math. Sci., **1**, pp. 59–67.
[36] Bastawrous, M. V., and Hussein, M. I., 2022, "Closed-Form Existence Conditions for Bandgap Resonances in a Finite Periodic Chain Under General Boundary Conditions," J. Acoust. Soc. Am., **151**(1), pp. 286–298.
[37] Sun, Y. M., Xing, J. C., Shao, L. H., and Wang, J. X., 2025, "The Topological Dynamics of Continuum Lattice Grid Structures," J. Mech. Phys. Solids, **194**, p. 105935.
[38] Chen, Y., Schneider, J. L. G., Wang, K., Scott, P., Kalt, S., Kadic, M., and Wegener, M., 2024, "Anomalous Frozen Evanescent Phonons," Nat. Commun., **15**(1), p. 8882.
[39] Willis, J. R., 2016, "Negative Refraction in a Laminate," J. Mech. Phys. Solids, **97**, pp. 10–18.
[40] Mokhtari, A. A., Lu, Y., Zhou, Q., Amirkhizi, A. V., and Srivastava, A., 2020, "Scattering of In-Plane Elastic Waves at Metamaterial Interfaces," Int. J. Eng. Sci., **150**, p. 103278.
[41] Lawrence, F. J., Botten, L. C., Dossou, K. B., De Sterke, C. M., and Mcphedran, R. C., 2009, "Impedance of Square and Triangular Lattice Photonic Crystals," Phys. Rev. A, **80**(2), p. 023826.
[42] Lawrence, F. J., Botten, L. C., Dossou, K. B., Mcphedran, R. C., and de Sterke, D. M. C., 2010, "Photonic-Crystal Surface Modes Found From Impedances," Phys. Rev. A, **82**(5), p. 053840.
[43] Xiao, M., Zhang, Z. Q., and Chan, C. T., 2014, "Surface Impedance and Bulk Band Geometric Phases in One-Dimensional Systems," Phys. Rev. X, **4**(2), p. 021017.
[44] Gao, W. S., Xiao, M., Chen, B. J., Pun, E. Y. B., Chan, C. T., and Tam, W. Y., 2017, "Controlling Interface States in 1D Photonic Crystals by Tuning Bulk Geometric Phases," Opt. Lett., **42**(8), p. 287737.
[45] Groß, M. F., Schneider, J. L. G., Wei, Y., Chen, Y., Kalt, S., Kadic, M., Liu, X. N., Hu, G. K., and Wegener, M., 2023, "Tetramode Metamaterials as Phonon Polarizers," Adv. Mater., **35**(18), p. 2211801.
[46] Chen, Y., Liu, X. N., and Hu, G. K., 2016, "Design of Arbitrary Shaped Pentamode Acoustic Cloak Based on Quasi-Symmetric Mapping Gradient Algorithm," J. Acoust. Soc. Am., **140**(5), pp. 405–409.
[47] Chang, Z., Guo, D. K., Feng, X. Q., and Hu, G. K., 2014, "A Facile Method to Realize Perfectly Matched Layers for Elastic Waves," Wave Motion, **51**(7), pp. 1170–1178.
[48] Sengsri, P., and Kaewunruen, S., 2020, "Additive Manufacturing Meta-Functional Composites for Engineered Bridge Bearings: A Review," Constr. Build. Mater., **262**, p. 120535.
[49] Allein, F., Anastasiadis, A., Chaunsali, R., Frankel, I., Boechler, N., Diakonos, F. K., and Theocharis, G., 2023, "Strain Topological Metamaterials and Revealing Hidden Topology in Higher-Order Coordinates," Nat. Commun., **14**(1), p. 6633.
[50] Chen, H., Nassar, H., and Huang, G. L., 2018, "A Study of Topological Effects in 1D and 2D Mechanical Lattices," J. Mech. Phys. Solids, **117**, pp. 22–36.
[51] Zhang, Q., and Rudykh, S., 2025, "Topological State Switches in Hard-Magnetic Meta-Structures," J. Mech. Phys. Solids, **196**, p. 106001.
[52] Shi, S., Xu, B., Zhang, K., Ye, G. S., Xiang, D. S., Liu, Y. B., Wang, J. Z., Su, D. Q., and Li, L., 2022, "High-Fidelity Photonic Quantum Logic Gate Based on Near-Optimal Rydberg Single-Photon Source," Nat. Commun., **13**(1), p. 4454.
[53] Prasad, R., and Sarkar, A., 2019, "Broadband Vibration Isolation for Rods and Beams Using Periodic Structure Theory," ASME J. Appl. Mech., **86**(2), p. 021004.
[54] Akbari-Farahani, F., and Ebrahimi-Nejad, S., 2024, "From Defect Mode to Topological Metamaterials: A State-of-the-Art Review of Phononic Crystals & Acoustic Metamaterials for Energy Harvesting," Sens. Actuators, A, **365**, p. 114871.
[55] Liu, H., Zhang, Q., Zhang, K., Hu, G. K., and Duan, H. L., 2019, "Designing 3D Digital Metamaterial for Elastic Waves: From Elastic Wave Polarizer to Vibration Control," Adv. Sci., **6**(16), p. 1900401.
[56] You, J. W., Ma, Q., Lan, Z. H., Xiao, Q., Panoiu, N. C., and Cui, T. J., 2021, "Reprogrammable Plasmonic Topological Insulators With Ultrafast Control," Nat. Commun., **12**(1), p. 5468.
[57] Assi, D. S., Huang, H. L., Karthikeyan, V., Theja, V. C. S., De Souza, M. M., Xi, N., Li, W. J., and Roy, V. A., 2023, "Quantum Topological Neuristors for Advanced Neuromorphic Intelligent Systems," Adv. Sci., **10**(24), p. 2300791.